SUPPORTING INFORMATION

Gated Single-Molecule Transport in Double-barreled Nanopores

Liang Xue[1], Paolo Cadinu[1], Binoy Paulose Nadappuram[1], Minkyung Kang[1], Ye Ma[1], Yuri Korchev[2], Aleksandar P. Ivanov[*1], Joshua B. Edel[*1]

1. Department of Chemistry, Imperial College London, Exhibition Road, London SW7 2AZ, UK
2. Department of Medicine, Imperial College London, London W12 0NN, UK

[*]Email: joshua.edel@imperial.ac.uk, alex.ivanov@imperial.ac.uk

Table of contents:

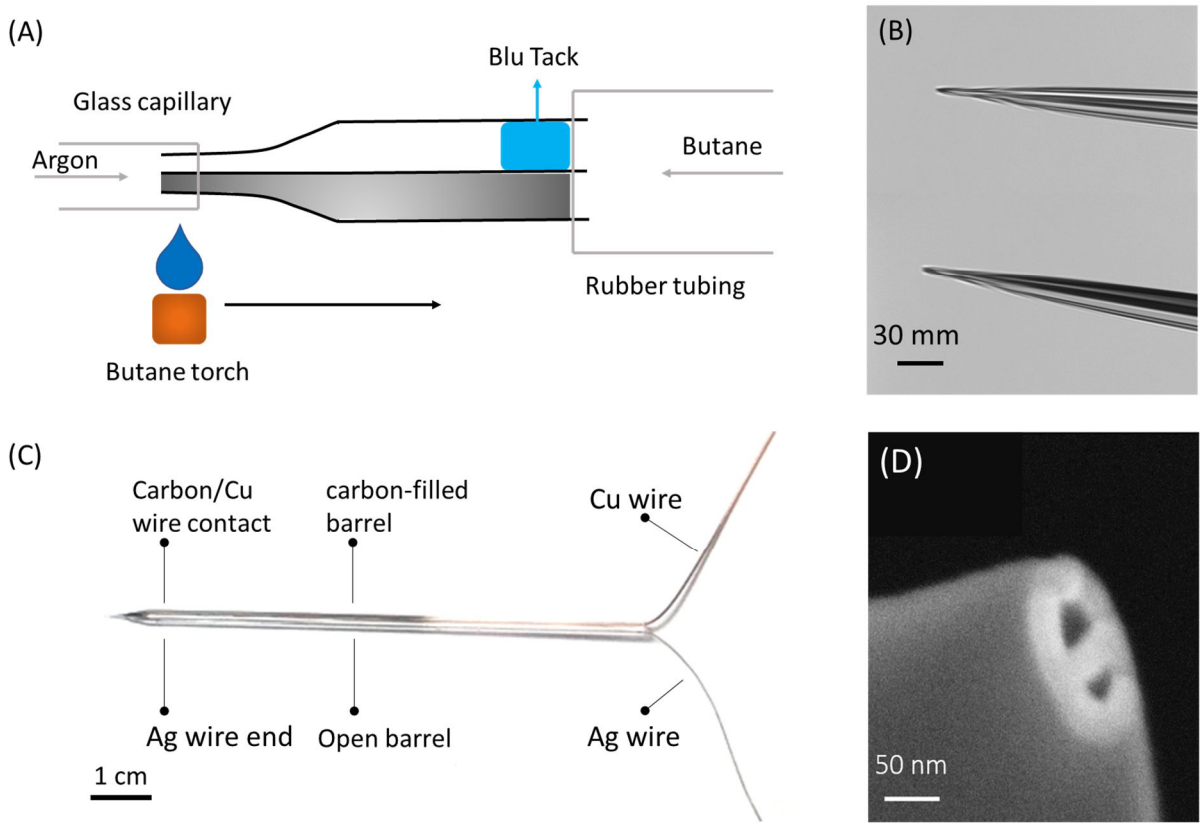

Figure S1: (A) Experimental set-up for pyrolytic deposition of carbon. Butane was passed through one barrel via a silicon tubing while the other barrel of the nanopipette was sealed. A butane torch was used to heat the tip of the pipette for pyrolytic deposition of carbon, under an argon flow to prevent further oxidation of deposited carbon. A heating time of 35 s was chosen to produce an extensive filament of amorphous carbon through one barrel while leaving another barrel open. (B) Bright-field micrograph showing a change in contrast between a dual-barrel nanopipette before and after carbon deposition. (C) Schematic demonstration of the electrical contact in a dual-barrel nanopipette with one barrel filled with carbon, the deposited carbon goes up to ~ 60 % of the nanopipette barrel. However, only the section at the taper of the nanopipette is extensively filled with carbon. The pyrolytic carbon is mostly deposited on the inner walls of the barrel to form a carbon layer. A copper wire was inserted into the carbon barrel so that it is embedded into the the bottom section just above the taper contacting directy the deposited carbon. (D) an SEM micrograph of a plain dual-barrel nanopipette before carbon deposition.

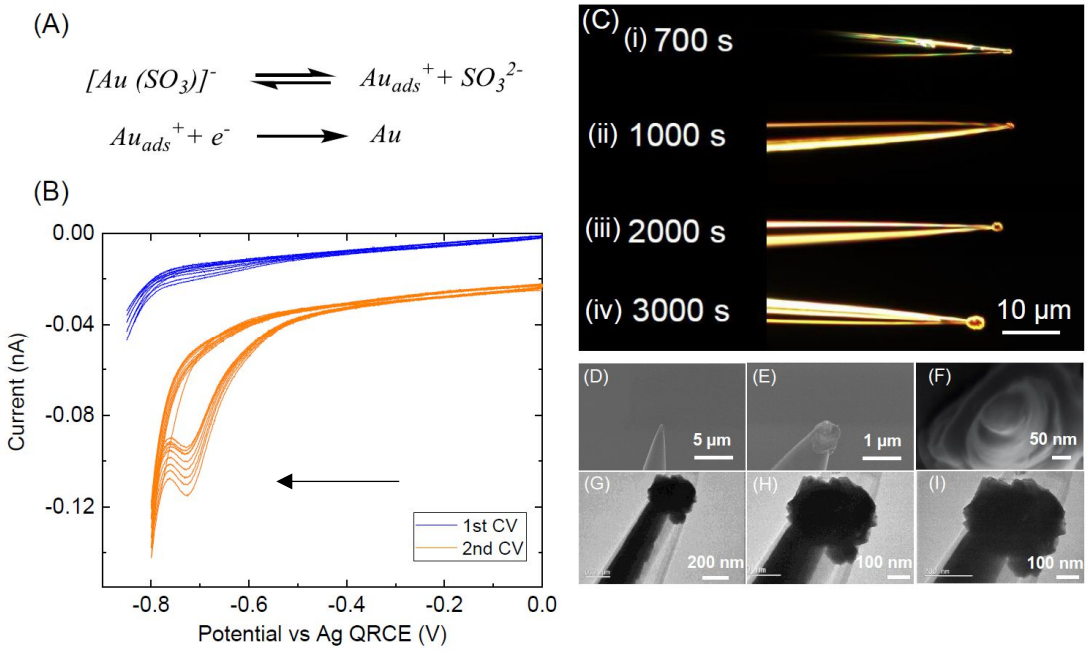

Figure S2: Gold deposition using an ECF64 plating solution on the carbon nanoelectrode. (A) Gold electrodeposition: the reaction proceeds via the dissociation of gold (I) complex on the electrode surface and the reduction of absorbed gold (I).[1] (B) Cyclic voltammograms of the carbon nanoelectrode in the gold plating solution before and after the amperometric deposition for 200 s at -0.73 V, illustrating an increase of electrode area with more gold deposited onto carbon. Scan rate = 0.2 V/s. (C) Dark-field images visualizing the growth of gold at the nanopipette tip after starting deposition for 700, 1000, 2000 and 3000 s. (D-F) SEM and (G-I) TEM images showing the localized gold structure around the nanopore opening after feedback-controlled gold deposition.

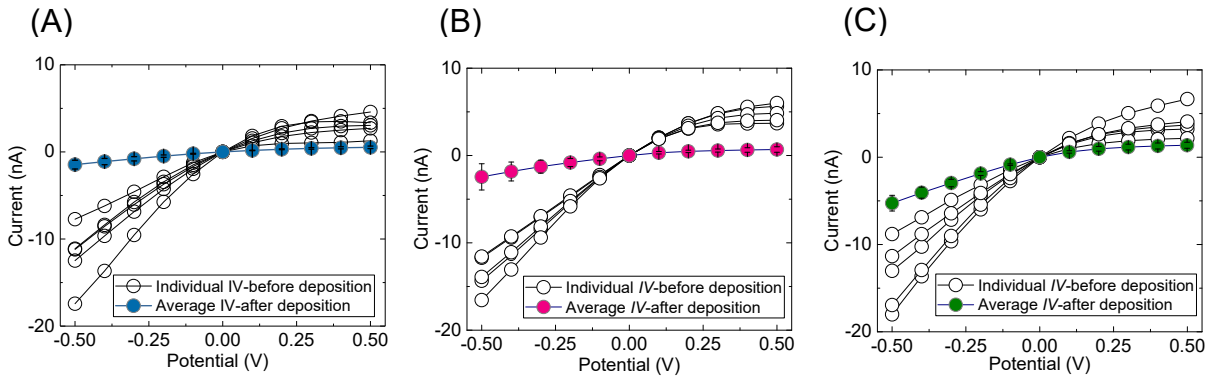

Figure S3: *I-V's* demonstrating the controllable decrease in nanopore dimensions using a threshold feedback current value of (A) -0.5 nA, (B) -1.0 nA and (C) -1.5 nA. *I-Vs* were recorded for 5 arbitrary selected nanopore devices. After feedback-controlled deposition of gold, the *I-Vs* were averaged and represented as the filled circles. Conductances were calculated by linear fits of the *I-Vs* in the ohmic region from -0.1V to 0.1 V. The average nanopore conductance before deposition was: 17.3 ± 6.4 nS and the average conductance for each threshold feedback current were as follows: 7.4 ± 0.2, 3.5 ± 1.9, and 1.9 ± 0.4 nS at -0.5, -1.0 and -1.5 nA, respectively. Error bars denote the standard deviation for N=5 different devices. All *I-V* characterization was performed in 52 mM $(NH_4)_2SO_3$.

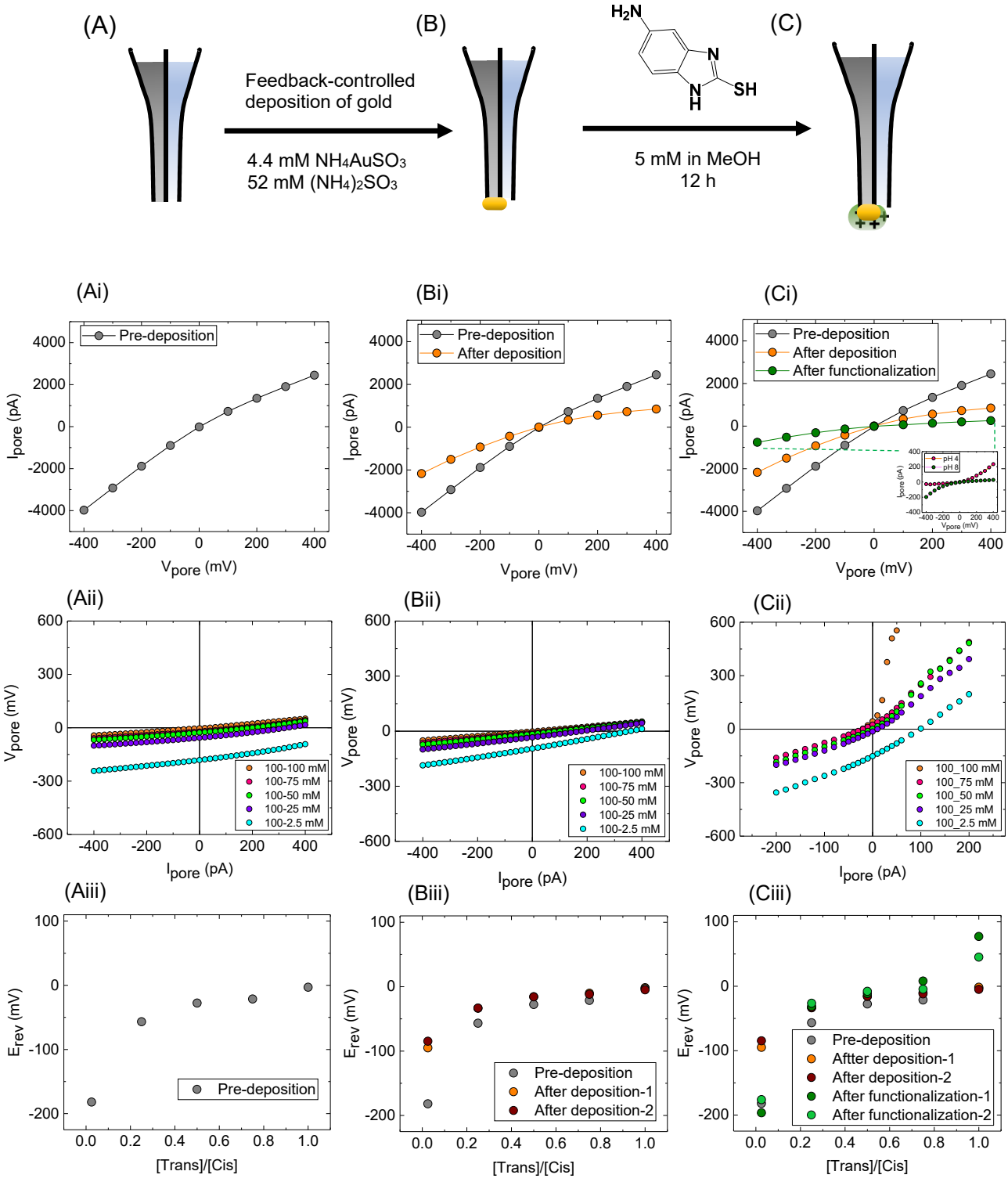

Figure S4: Fabrication process of the nanopore-FET device, starting from (A) unmodified (carbon only) pipettes, to (B) gold modified pipettes, and then (C) functionalized pipettes, with the corresponding (i) *I-V* characterization after each stage of fabrication. Conductance values in 100 mM KCl were 8.13 ± 0.43 nS before deposition, 3.79 ± 0.30 nS after deposition, and 1.00 ± 0.15 nS after functionalization. Considering the change of the nanopore surface charge after amine functionalization, the *I-V* response across the nanopore, revealed a significant change from negative to positive rectification by tuning the

pH from 8 to 4 in 10 mM KCl (inset, ciii). (ii) Ion selectivity measurements across nanopores after each stage of fabrication, by using current clamp mode of a Multiclapm 700B amplifier. Potential-current (I-clamp) measurements for nanopore-FET devices (A) before deposition, (B) after deposition and (C) after functionalization at different KCl concentration gradients. The concentration of KCl was only diluted outside of the nanopore. (iii) The potential at which the current is set to zero is represented as the reversal potential (E_{rev}). Before deposition, the nanopores exhibited cationic selectivity, indicated by (Aiii) more negative reversal potentials as the concentration of trans side is diluted. (Biii) After deposition, the reversal potentials became less negative, due to the reduction of surface charge. (Ciii) The appearance of more positive reversal potentials after amine functionalization indicated more positive nanopore surface charge. Ion-selectivity measurements showed a gradual tuning of nanopore surface charge. In all cases, the gate electrode was left floating. *I-V* (V-clamp) characterization was performed in 100 mM KCl, 10 mM Tris-HCl and 1 mM EDTA buffer at pH 8. Potentials quoted here are relative to Ag/AgCl reference electrode in KCl bath.

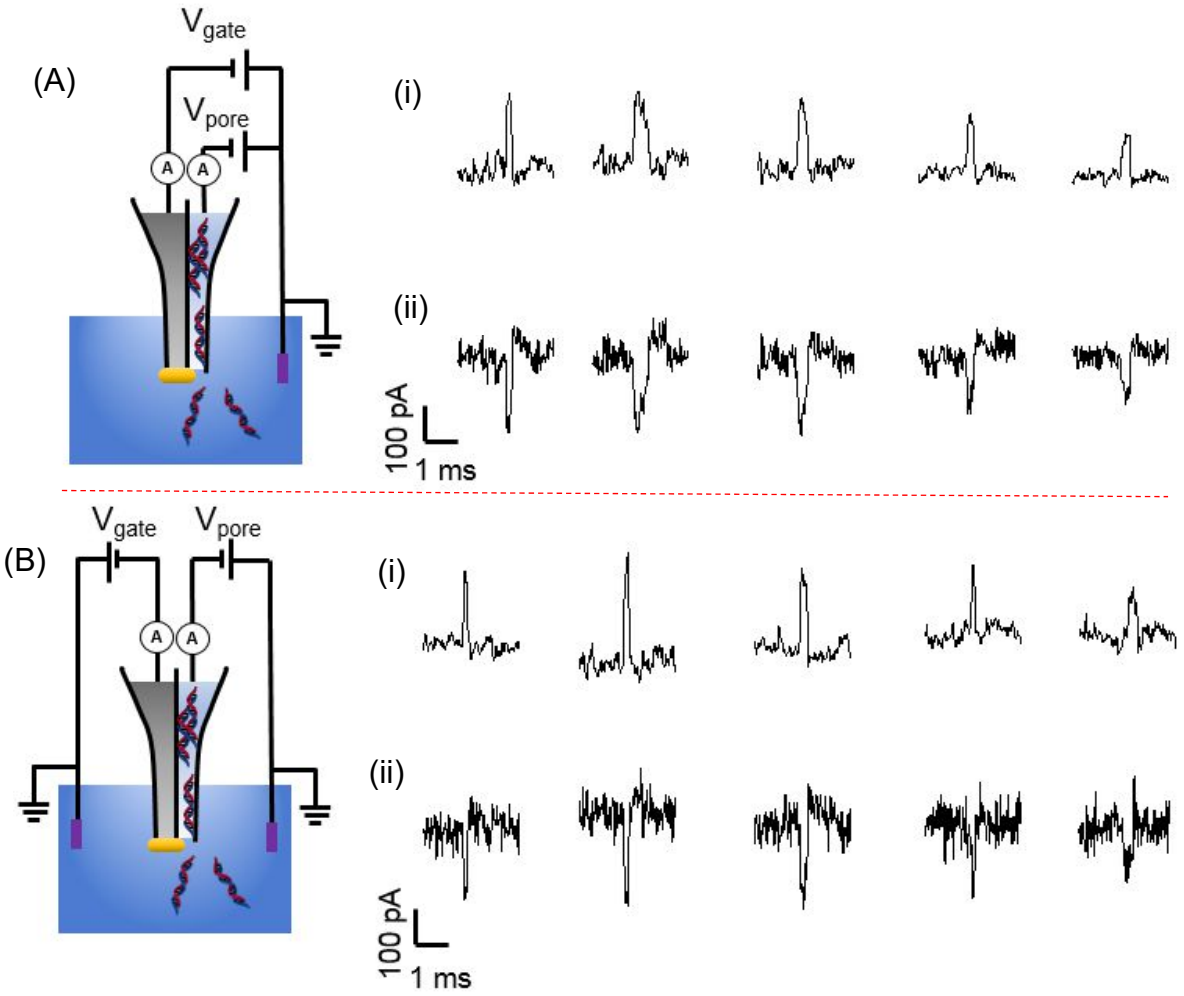

Figure S5: Comparison of single-molecule translocation events using (A) a single Ag/AgCl reference electrode (linked reference electrodes) and (B) a dual independent reference Ag/AgCl electrode. The representative translocation peaks show individual translocation event detected at (i) the nanopore channel (upper panel) and (ii) the gate channel (lower panel). These results showed a negligible difference for using single reference electrode or dual reference electrode in KCl bath. Experimental conditions: 100 mM KCl in 10 mM Tris-HCl and 1 mM EDTA buffer, with 400 pM of 10 kbp DNA added inside of nanopipette. V_{pore}= -700 mV, V_{gate} = 0 mV.

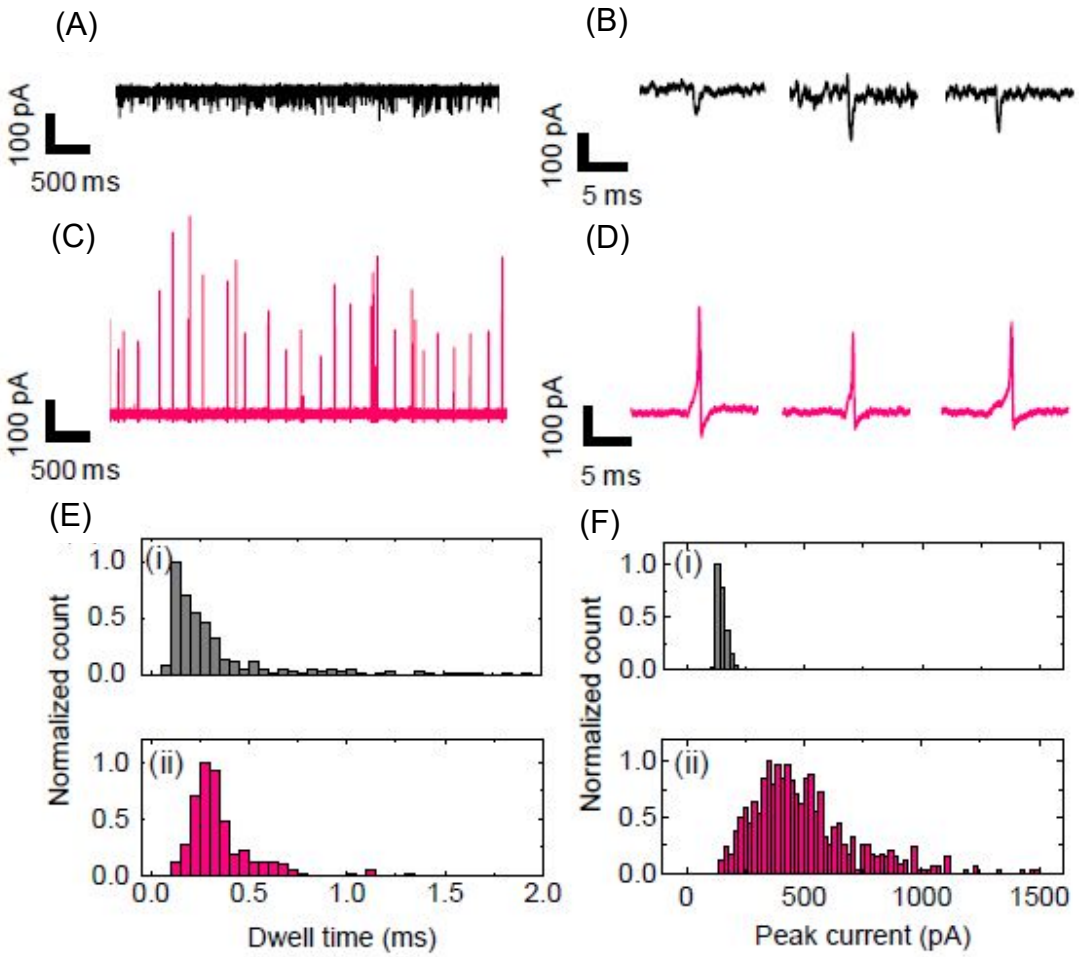

Figure S6: Validation of single-molecule functionality for the nanopore-FET devices. Representative *I-t* traces and individual translocation events recorded at the nanopore channel (A,B) before and (C,D) after feedback-controlled deposition of gold, showing there is a slight increase of the dwell time from (Ei) 0.13 ± 0.06 ms to (Eii) 0.35 ± 0.17 ms, and a significant increase of peak current from (Fi) 149 ± 25 pA to (Fii) 510 ± 252 pA, and a reduction of capture rate from 17 ± 3 s^{-1} to 7 ± 1 s^{-1}. This was attributed to the smaller opening of the gold-coated nanopore which induced enhanced interactions between DNA and nanopore surface. V_{pore} = -700 mV, V_{gate} = 0 mV.

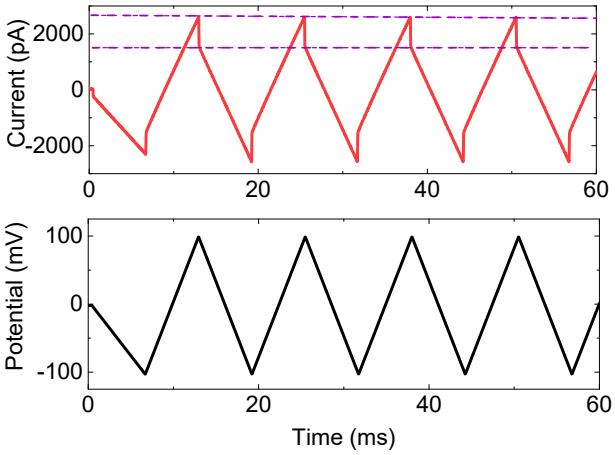

Figure S7: Capacitance and resistance of the nanopore-FET devices. Representative *I-t* traces used for the estimation of capacitance and resistance for the nanopore and the gate channel. Using a similar protocol to the one described Balan et al.[2], a 100 Hz triangle wave from -100 to 100 mV was applied to the nanopore or the gate channel. The capacitance was estimated from current steps when the slope of applied potential changes sign. The resistance was obtained by linearly fitting *I-t* trace from -50 to 50 mV. All measurements were performed in 100 mM KCl, 10 mM Tris-HCl and 1 mM EDTA buffer, at pH 8.

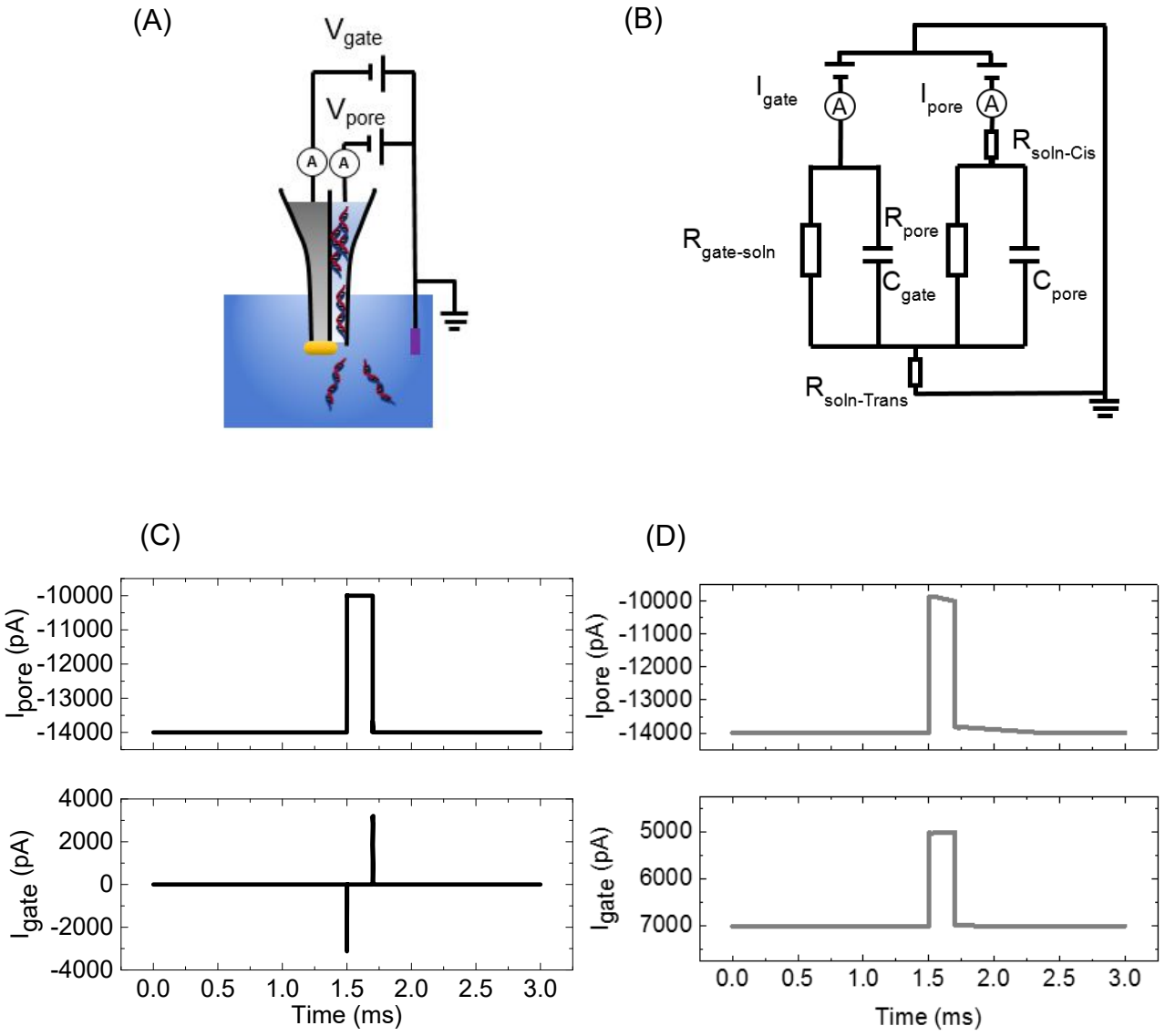

Figure S8: Circuit simulation for a nanopore-FET device. (A) Schematic illustration of experimental set-up and (B) an equivalent electric circuit for measuring single-molecule DNA translocations by nanopore-FET devices. Single-molecule translocations were modeled by as a pulse change of nanopore resistance with a duration of 0.25 ms. (C) Based on measured values of capacitance and resistance at 100 mM KCl, simulated results showed a biphasic response from the gate. The gate resistance R_{gate} (200 MΩ) was much larger than solution resistance R_{soln} (1.84 kΩ). (D) When R_{gate} (1.84 kΩ) becomes comparable to R_{soln} (1.84 kΩ), current leakage occurs from nanopore to the gate. In this case, the shape of the simulated translocation events I_{gate} mirrored those at the nanopore channel I_{pore}.

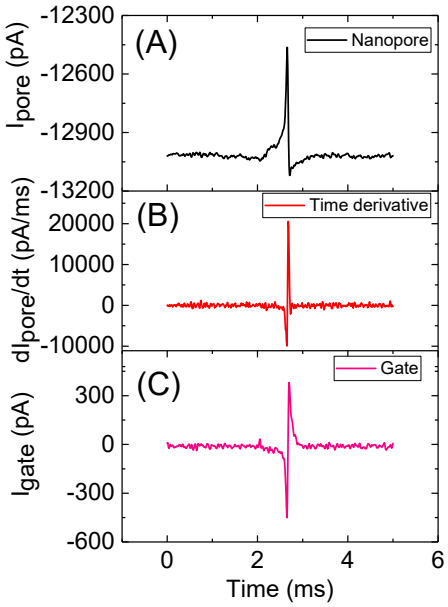

Figure S9: Correlating biphasic response from the gate with the time derivative of the nanopore translocation peak current**.** An example of a single-molecule DNA translocation event measured (A) at the nanopore channel, and (B) subsequent analysis by calculating the time derivative of this event, showing a reasonable match with (C) the actual biphasic peak on the gate. V_{pore} = -700 mV, V_{gate} = 0 mV.

To elucidate this synchronized biphasic response from gate to single-molecule DNA translocation events from the nanopore, the following derivations were performed.

1) the ionic current flowing through nanopore changes as a result of single-molecule DNA translocation.
2) the change of ionic current produces a transient change of electric potential around the gate.
3) a transient current is measured at the gate due to the change of electric potential.

$$I_{gate} = \frac{dq}{dt} \quad (1)$$

$$q = C_{gate} V_{gate} \quad (2)$$

$$dq = -C_{gate} dV_{gate} \quad (3)$$

Substitute (3) into (1):

$$I_{gate} = C_{gate} \frac{dV_{gate}}{dt} \quad (4)$$

Ohm's law:

$$V = IR \quad (5) \rightarrow dV = RdI \text{ at a constant } R \quad (6)$$

For our case:

$$dV_{gate} = R_{gate} dI_{pore} \quad (7)$$

Substitute (7) into (4):

$$I_{gate} = -C_{gate} R_{gate} \frac{dI_{pore}}{dt} \quad (8)$$

From equation 8, the synchronized response appears to be the time derivative of ionic current from nanopore. The latter can be confirmed by calculating the time derivative of translocation peaks from nanopore. A comparison of the derivative current with the original current measured at the gate revealed a close match of their biphasic shapes.

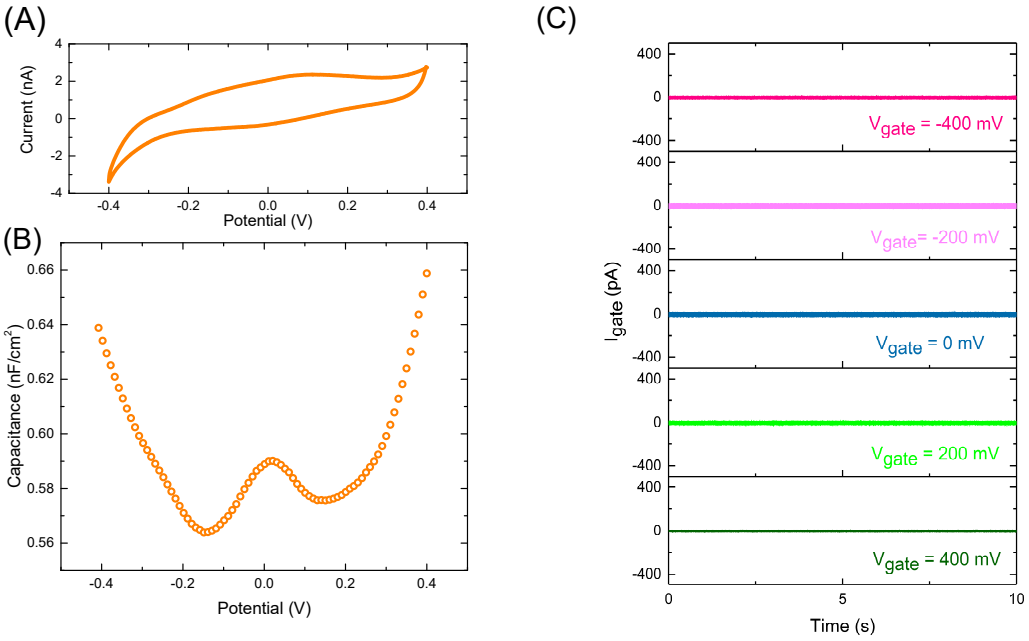

Figure S10: Electrochemical characterization of an amine-modified ultramicro gold electrode (A) cyclic voltammetry from -0.4 to 0.4 V showed minimal faradic currents within the range of V_{gate}, scan rate = 0.2 V/s. (B) Differential capacitance measurements of an amine modified electrode showed a secondary capacitance minimum at 0.15 V. Effective charge tuning at the electrode/electrolyte interface was obtained for the functionalized system, as seen from the pronounced change of capacitance at both sides of the point of zero charge; Using a nanopore-FET, (C) *I-t* traces recorded from amine functionalized gate showed that the magnitude of current remained at 0 pA, indicating that is unlikely that Faradaic processes taking place on the functionalized gate electrode in the potential window V_{gate} = -400 to V_{gate} = 400 mV. All characterization was performed in 100 mM KCl, 10 mM Tris-HCl and 1 mM EDTA buffer at pH 8.

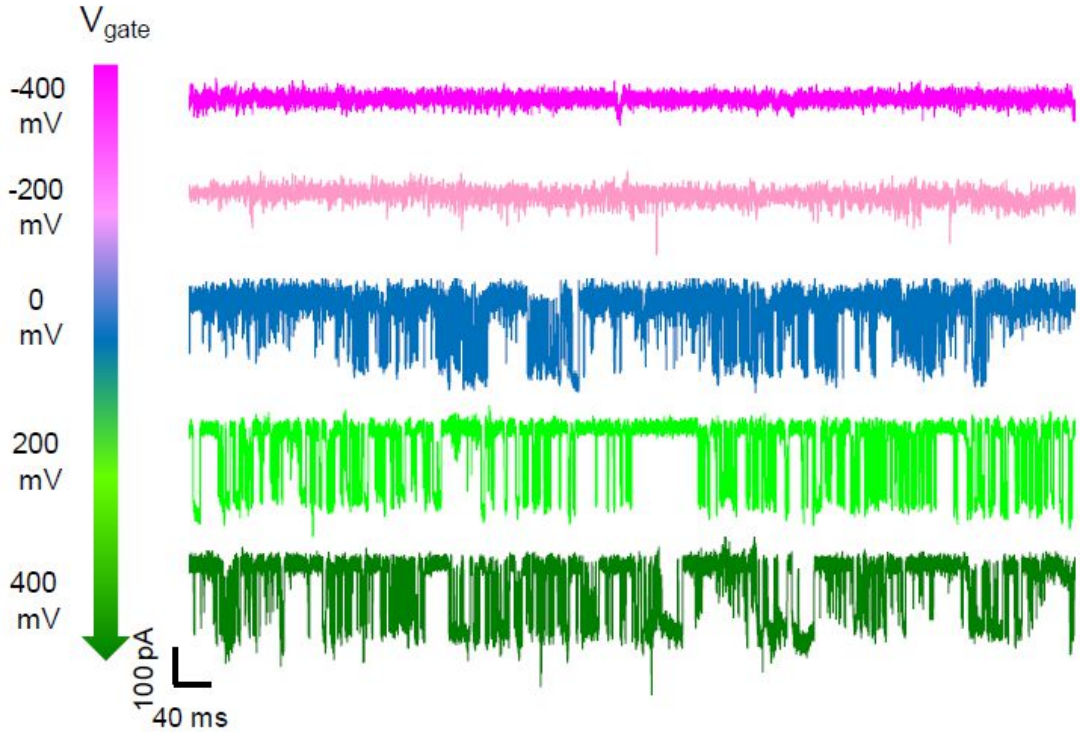

Figure S11: Supplementary traces of 10 kbp DNA confirming the reproducibility of voltage gating with amine-functionalized nanopore-FETs. V_{pore} = -500 mV. V_{gate} was tuned between -400 and 400 mV.

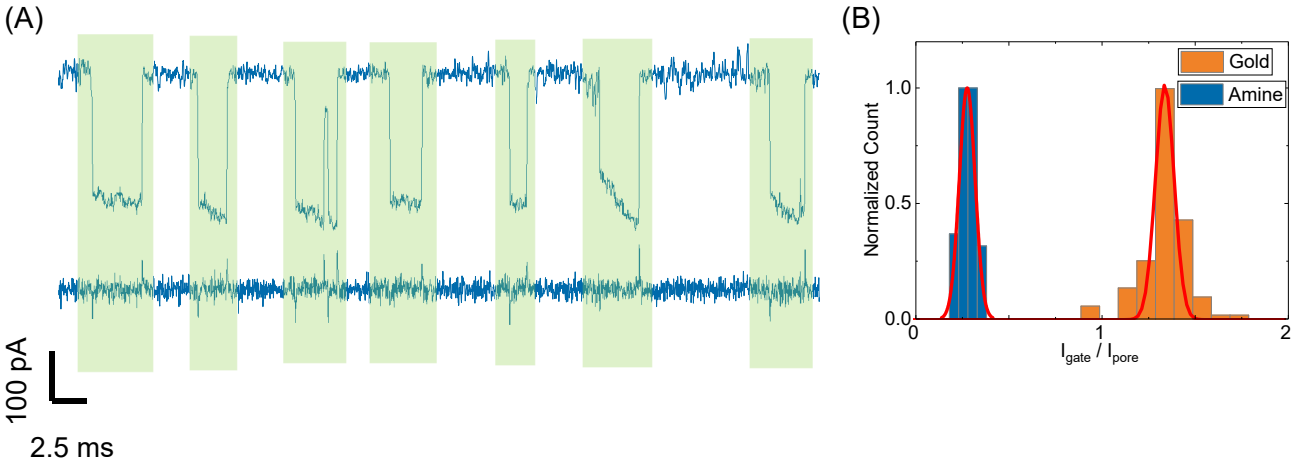

Figure S12: Synchronized detection of single-molecule DNA translocations using an amine functionalized nanopore-FET device. (A) Dual-channel detection from nanopore (upper panel) and the gate (lower panel) after amine functionalization. (B) Compared to gold nanopore-FET devices, the amine functionalized device exhibited elongated separation of biphasic peaks and a lower ratio of I_{gate}/I_{pore} (1.37 ± 0.16 for gold device, 0.28 ± 0.04 for amine-modified device), due to an additional positively charged coating that slows down DNA translocation. Experimental conditions: 100 mM KCl in 10 mM Tris-HCl and 1mM EDTA buffer, pH 8, with 200 pM of 10 kbp DNA being added inside of nanopipette. V_{pore} = -500 mV, V_{gate} = 0 mV.

References

(1) Osaka, T.; Kato, M.; Sato, J.; Yoshizawa, K.; Homma, T.; Okinaka, Y.; Yoshioka, O. Mechanism of Sulfur Inclusion in Soft Gold Electrodeposited from the Thiosulfate-Sulfite Bath. *J. Electrochem. Soc.* **2001**, *148*, C659–C662.

(2) Balan, A.; Machielse, B.; Niedzwiecki, D.; Lin, J.; Ong, P.; Engelke, R.; Shepard, K. L.; Drndic, M. Improving Signal-to-Noise Performance for DNA Translocation in Solid-State Nanopores at MHz Bandwidths. *Nano Lett.* **2014**, *14*, 7215–7220.